NASA/TM-20210024918

A Study of Highly Underexpanded Supersonic Jets in Subsonic Crossflow

Ryan D. Schindler
University of Toledo, Toledo, Ohio

Raymond S. Castner and Khairul B.M.Q. Zaman
Glenn Research Center, Cleveland, Ohio

February 2022

NASA STI Program . . . in Profile

Since its founding, NASA has been dedicated to the advancement of aeronautics and space science. The NASA Scientific and Technical Information (STI) Program plays a key part in helping NASA maintain this important role.

The NASA STI Program operates under the auspices of the Agency Chief Information Officer. It collects, organizes, provides for archiving, and disseminates NASA's STI. The NASA STI Program provides access to the NASA Technical Report Server—Registered (NTRS Reg) and NASA Technical Report Server—Public (NTRS) thus providing one of the largest collections of aeronautical and space science STI in the world. Results are published in both non-NASA channels and by NASA in the NASA STI Report Series, which includes the following report types:

- TECHNICAL PUBLICATION. Reports of completed research or a major significant phase of research that present the results of NASA programs and include extensive data or theoretical analysis. Includes compilations of significant scientific and technical data and information deemed to be of continuing reference value. NASA counter-part of peer-reviewed formal professional papers, but has less stringent limitations on manuscript length and extent of graphic presentations.

- TECHNICAL MEMORANDUM. Scientific and technical findings that are preliminary or of specialized interest, e.g., "quick-release" reports, working papers, and bibliographies that contain minimal annotation. Does not contain extensive analysis.

- CONTRACTOR REPORT. Scientific and technical findings by NASA-sponsored contractors and grantees.

- CONFERENCE PUBLICATION. Collected papers from scientific and technical conferences, symposia, seminars, or other meetings sponsored or co-sponsored by NASA.

- SPECIAL PUBLICATION. Scientific, technical, or historical information from NASA programs, projects, and missions, often concerned with subjects having substantial public interest.

- TECHNICAL TRANSLATION. English-language translations of foreign scientific and technical material pertinent to NASA's mission.

For more information about the NASA STI program, see the following:

- Access the NASA STI program home page at http://www.sti.nasa.gov

- E-mail your question to help@sti.nasa.gov

- Fax your question to the NASA STI Information Desk at 757-864-6500

- Telephone the NASA STI Information Desk at 757-864-9658

- Write to:
  NASA STI Program
  Mail Stop 148
  NASA Langley Research Center
  Hampton, VA 23681-2199

NASA/TM-20210024918

A Study of Highly Underexpanded Supersonic Jets in Subsonic Crossflow

Ryan D. Schindler
University of Toledo, Toledo, Ohio

Raymond S. Castner and Khairul B.M.Q. Zaman
Glenn Research Center, Cleveland, Ohio

National Aeronautics and
Space Administration

Glenn Research Center
Cleveland, Ohio 44135

February 2022

Acknowledgments

The authors thank Dr. Amy F. Fagan for help in various forms throughout the study, Christopher Heath for help with the FUN3D algorithm, and other members of the Inlets and Nozzles Branch at the NASA Glenn Research Center for assistance with the numerical work. Ryan D. Schindler thanks the Lewis' Educational and Research Collaborative Internship Project (LeRCIP) for support. Support for this project was provided by Commercial Supersonic Technology (CST) Project of NASA's Advanced Air Vehicles Program.

This work was sponsored by the Advanced Air Vehicle Program
at the NASA Glenn Research Center

Level of Review: This material has been technically reviewed by technical management.

Available from

NASA STI Program
Mail Stop 148
NASA Langley Research Center
Hampton, VA 23681-2199

National Technical Information Service
5285 Port Royal Road
Springfield, VA 22161
703-605-6000

This report is available in electronic form at http://www.sti.nasa.gov/ and http://ntrs.nasa.gov/

A Study of Highly Underexpanded Supersonic Jets in Subsonic Crossflow

Ryan D. Schindler*
University of Toledo
Toledo, Ohio 43606

Raymond S. Castner and Khairul B.M.Q. Zaman
National Aeronautics and Space Administration
Glenn Research Center
Cleveland, Ohio 44135

Abstract

Numerical and empirical solutions were compared to experimental results for under-expanded supersonic jets penetrating normally into a subsonic crossflow. The injector jet trajectory was determined experimentally through Pitot probe surveys. Numerical solutions were obtained through FUN3D (a 3-D Unstructured Navier Stokes solver) for nine cases where the injector 'jet Mach number' ranged from 1.38 to 3.29 while the crossflow was maintained at a constant Mach number of 0.275. Four different turbulence models were used in the numerical study: Spalart-Allmaras (SA), Shear-Stress-Transport (SST), 'SA-Neg', and 'SST-V'. At a low supersonic jet Mach number, the four turbulence models produced similar results. At higher Mach numbers, only the SA produced a converged solution, however, the numerically determined jet trajectories deviated noticeably from the experimental data as the injector jet Mach number increased. The numerical and experimental results were compared to four empirical formulae found in the literature. All four were inadequate in predicting the jet trajectories for the operating conditions reported in this study. Two of the empirical formulae were modified to bring the predictions within reasonable agreement with the experimental data.

Nomenclature

d	diameter of the injector jet orifice
J	Momentum Flux Ratio = $\frac{\rho_{ij} U_{ij}^2}{\rho_{cf} U_{cf}^2}$
ρ_{ij}	injector jet density at orifice exit
U_{ij}	injector jet velocity
ρ_{cf}	crossflow density
U_{cf}	crossflow velocity
r	effective velocity ratio = $J^{1/2}$
γ	ratio of specific heats
h	vertical portion of the injector jet trajectory before bending
C_m	proportionality constant
δ	boundary layer thickness

*Summer Intern with Lewis' Educational and Research Collaborative Internship Project (LeRCIP), 2016, at NASA Glenn Research Center

d_j fully-expanded injector jet plume diameter
M_{ij} fully-expanded injector jet Mach number
M_{cf} Crossflow Mach number
M_e Injector jet Mach number at exit
Ps static pressure
Po stagnation pressure
A,B,α,β constants

1.0 Introduction

A jet in cross flow (JICF) refers to an injector jet exhausting from an orifice into a transverse cross flow. The JICF configuration occurs in many engineering applications such as for air fuel mixing, boundary layer separation control, film-cooling, etc. An ability to predict the injector jet trajectory is critical in many of these applications. This study investigates the jet trajectory of a highly underexpanded supersonic JICF, covering a flow regime that received little attention in past studies. Experimental and numerical results are compared with empirical formulae available from the literature, in an effort to assess and improve the prediction capabilities of such JICF trajectories.

As the injector jet penetrates the crossflow, it bends in the direction of the crossflow and various types of vortices are formed: counter-rotating vortex pair (CVP), horseshoe or necklace vortices, wake vortices, and shear layer vortices. These vortices are described in numerous previous studies (Refs. 1 to 7) and some of the features are shown in Figure 1, taken from Beresh et al. (Ref. 2). Detailed measurements of the CVP have been performed by Kamotani & Greber (Ref. 3) and Fearn & Weston (Ref. 4). Horseshoe vortices were investigated by Krothapalli, Lourenco and Buchlin (Ref. 5) and by Kelso and Smits (Ref. 6). The structure of the wake vortices was analyzed by Fric and Roshko (Ref. 7).

Many other aspects of JICF have been studied in the past. Zaman (Ref. 1), for example, reviewed unsteady JICF with periodic perturbation. While the majority of past studies covered subsonic flow regimes, some covered high Mach number flows. Foster and Engblom (Ref. 8) investigated injection into supersonic crossflow with various orifice geometries. Papamoschou and Hubbard (Ref. 9) studied the interaction between supersonic injectors and supersonic crossflow.

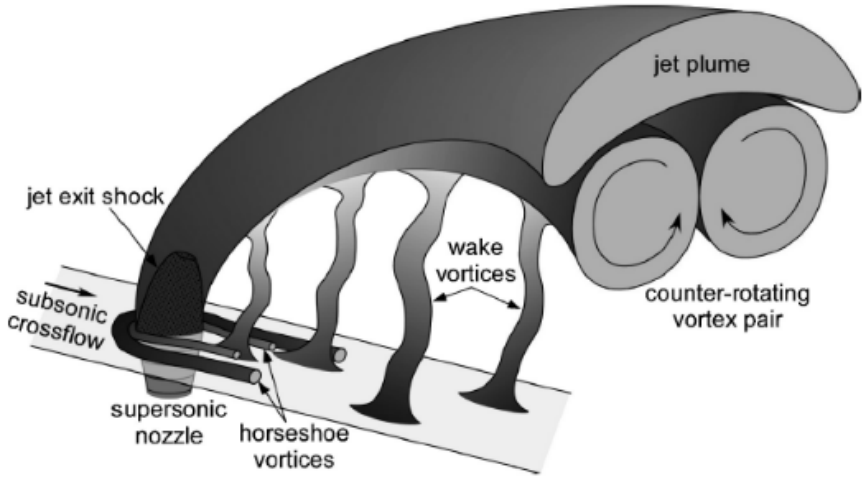

Figure 1.—Injector jet flow showing various vortex structures, from Reference 2.

Previous JICF studies developed formulae to estimate the injector jet plume trajectory. Abramovich (Ref. 10) defined the trajectory as,

$$\frac{z}{d} = \left(\frac{x}{d}\right)^{\frac{1}{3}} J^{\frac{1.3}{3}} \tag{1}$$

where z is the trajectory height, d is the orifice diameter, x is the distance downstream of the crossflow nozzle exit, and J is the momentum flux ratio. Karagozian (Ref. 11) explored the vortices associated with transverse jets and developed an analytical solution to predict the trajectory of the CVP as,

$$\frac{z}{d} = \alpha(r)^{\beta}\left(\frac{x}{d}\right)^{\gamma} \tag{2}$$

where α, β, γ are constants with values of 1.50, 0.27, and 0.37, respectively, and $r = \sqrt{J}$. Broadwell and Breidenthal (Ref. 12) derived a formula to predict the jet trajectory by treating the injector exit as a point source of momentum. The resulting formula is given by,

$$\frac{z}{rd} = A\left(\frac{x}{rd}\right)^{B} \tag{3}$$

where A and B are constants. Margason (Ref. 13) defined the ranges of the constants as $1.2 < A < 2.6$ and $0.28 < B < 0.34$. Muppidi and Mahesh (Ref. 14) investigated previously developed trajectory formulae and derived their own prediction by incorporating the portion of the jet that remains vertical before bending in the direction of the crossflow. Their formula is given by,

$$\frac{z}{rd} = A\left(\frac{x}{rd}\right)^{B}\left(\frac{h}{d}\right)^{0.15} \tag{4}$$

where h/d is the vertical portion of the jet which is defined by the piecewise functions,

$$\begin{cases} \dfrac{h}{d} = \left(\dfrac{3}{4}\pi C_m r^2 \dfrac{\delta^2 d_j^2}{d^4}\right)^{\frac{1}{3}} \text{ when } h \le \delta \\ \dfrac{h}{d} = \dfrac{2}{3}\dfrac{\delta}{d} + \dfrac{\pi}{4} C_m r^2 \dfrac{d_j^2}{d^2} \quad \text{when } h \ge \delta \end{cases} \tag{5}$$

Here, C_m is the proportionality constant and d_j is the effective jet plume diameter. For an underexpanded jet, the effective jet diameter is given by,

$$\frac{d_j}{d} = \frac{1 + \frac{1}{2}(\gamma - 1) M_{ij}^2}{1 + \frac{1}{2}(\gamma - 1) M_e^2}^{\frac{\gamma+1}{4(\gamma-1)}} \left(\frac{M_e}{M_{ij}}\right)^{\frac{1}{2}} \tag{6}$$

where M_e is the Mach number at the exit of the injector and M_{ij} is the fully expanded jet Mach number (Tam and Tanna (Ref. 15)).

In this study, experiments are conducted for underexpanded injector jets exhausting into a subsonic crossflow. This is accompanied by limited numerical simulations. Empirical formulae for the jet trajectory are compared with the experimental and numerical results. Two of the empirical formulae are modified to fit the current results. The Experimental Procedure is described in Section 2.0. Section 3.0 describes the Numerical Methods. Results are given in Section 4.0, followed by conclusion and summary in Section 5.0.

2.0 Experimental Procedure

An open jet facility (CW17) at the NASA Glenn Research Center was used for the experimental investigation. Compressed air passed through a 30 in. diameter plenum chamber before exhausting through the nozzle in quiescent air of the test chamber. An 8:1 aspect ratio rectangular nozzle, referred to as 'NA8Z' (Ref. 16), was used to produce the crossflow. The nozzle exit has dimensions of 5.34 by 0.66 in. and thus an equivalent diameter of 2.12 in.; detailed coordinates for the nozzle, suitable for adaptation in numerical simulation, can be found in References 16 and 17. The flow from the nozzle exhausted over a 1/2 in.-thick 24 in.-wide aluminum plate that was 8 in. long in the streamwise direction (Figure 2). The plate was aligned with the nozzle's long edge.

The injector jet exhausted through a 0.02 in. diameter orifice in the plate, located centrally with respect to the nozzle's major dimension and 0.46 in. downstream from the nozzle exit. The orifice had a depth of 0.125 in. and connected to a bigger diameter recess at the bottom of the plate that was supplied with compressed air from a K-bottle. Coordinates x, y and z denote streamwise, lateral (horizontal) and transverse (vertical) distances, respectively, with the origin at the center of the orifice exit.

In all experiments, the crossflow jet Mach number was maintained at 0.275. The flow was unheated. The fully expanded Mach number of the injector jet, computed from the ratio of the jet stagnation pressure to the ambient pressure, ranged from 1.32 to 3.29. Flow field surveys by a Pitot probe were conducted. The probe (Figure 2) was used to determine the location of the maximum velocity along the center plane ($y = 0$). The probe was traversed along z-axis to locate the maximum velocity point (corresponding to maximum Pitot pressure) at a given downstream location (x). The probe traverser had a resolution of 0.001 in. The jet trajectory was defined as the curve connecting the points of maximum velocity.

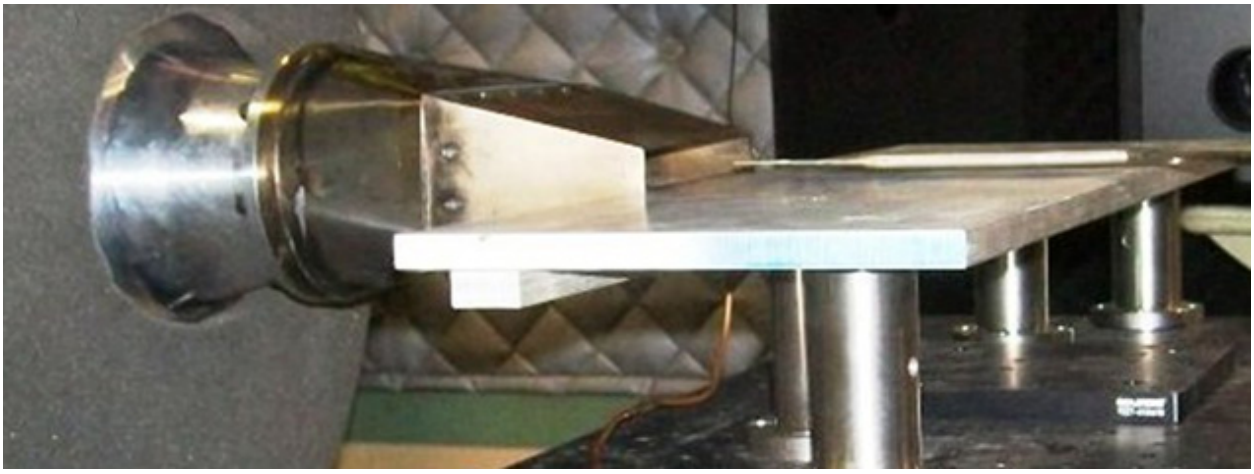

Figure 2.—A photograph of the experimental set-up showing the jet nozzle supplying the cross-flow along a flat plate. An orifice in the plate, supplied with compressed air from underneath, produces the JICF. A Pitot probe can be seen above the plate.

3.0 Numerical Methods

The experimental set-up was recreated in the mesh generating software POINTWISE V17.3R4 as shown in Figure 3 and Figure 4. From the center of the injector orifice, the outer domain extended in the downstream direction 153*d*. The model for the rectangular jet nozzle was imported into POINTWISE from SolidWorks. The surface mesh was generated within Pointwise. The volume mesh was built by AFLR3, an unstructured volume mesh generator. NASA's FUN3D code (Ref. 18), a fully unstructured Navier-Stokes 3-D flow solver, was used to obtain the flow solutions. FUN3D's adjoint-based mesh adaptation tool was used to generate the volume grids. The adjoint mesh is capable of stretching and orienting the grid based on error estimations of pressure in the solution space (Ref. 18). Figure 5 shows a view of the symmetry plane with the mesh created by the adjoint-based mesh adaptation. The total volume cell counts for the lowest and highest jet Mach number cases were 4.8×10^7 and 5.3×10^7, respectively. Nine test cases were investigated using the Spalart-Allmaras (SA) turbulence model for injector jet Mach numbers from 1.38 to 3.29. The test cases were then investigated using FUN3D's Negative Spalart-Allmaras (SA-Neg), Shear Stress Transport (SST), and Shear Stress Transport Vorticity (SST-V) turbulence models.

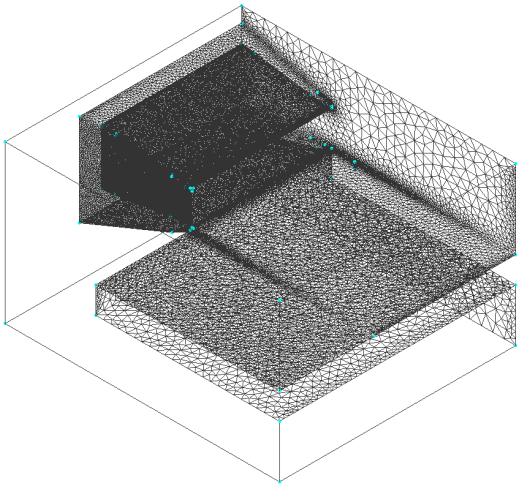

Figure 3.—An orthogonal view of the computational domain created in POINTWISE.

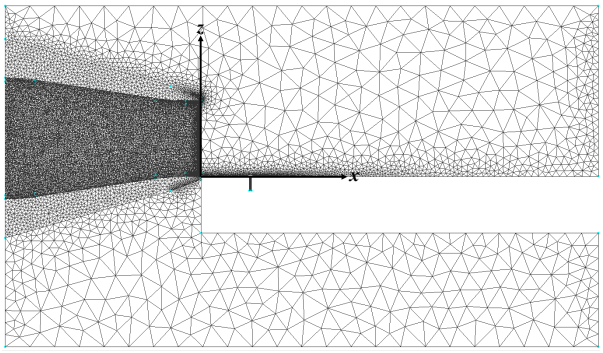

Figure 4.—A Side view of the computational domain created in POINTWISE.

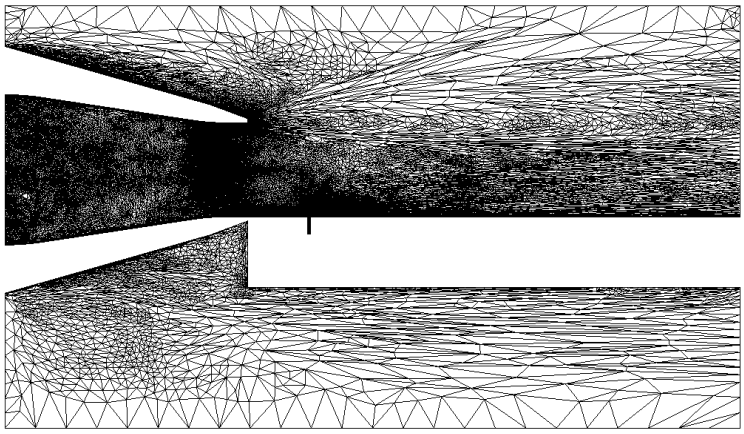

Figure 5.—The final grid obtained from FUN3D's feature and adjoint-based mesh adaptation.

4.0 Results

4.1 Experimental Results

The experimental results are presented here and compared with the empirical formulae. The formulae developed by Abramovich (Ref. 10), Karagozian (Ref. 11), Broadwell and Breidenthal (Ref. 12), and Muppidi and Mahesh (Ref. 14) are explored. Shown in Figure 6 are the comparisons between the experimental data and predictions from Abramovich. The predictions underestimate the penetration of the injector jet for $M_{ij} < 2$ and overestimate the penetration for $M_{ij} > 2$. The difference between the predicted and measured values increases with increasing Mach number.

The comparisons between the experimental data and Karagozian's correlation are shown in Figure 7. Relative to the predictions with Abromovich's formula, Karogozian's correlation produces a smaller initial ($x/d < 4$) jet penetration at higher values of M_{ij}, and overall a better agreement with the data. However, it can be seen that the predictions underestimate the jet penetration for all injector Mach numbers when x/d is larger than 7.

The empirical formula determined by Broadwell and Breidenthal (Ref. 12) included two constants (A and B) with ranges of A and B specified. When comparing the formula to the experimental results the predictions underestimated the initial injector trajectory. In order to bring the predictions within reasonable agreement of the experimental results the constants had to be extended beyond their specified ranges. New values for the constants were determined from the experimental data and best fit curves were generated to give the values for A and B as,

$$A = 0.0025\left(r^2\right) - 0.0677\left(r\right) + 1.7951 \tag{7}$$

and

$$B = -0.0006\left(r^2\right) + 0.0225\left(r\right) + 0.2639 \tag{8}$$

The values for A and B which match the experimental data along with the best-fit curves (Eqs. (7) and (8)) are shown in Figure 8. These values of A and B accurately represent the jet trajectory having an error less than 5 percent for all values of z/d. Note that the fitted curves have sharp gradients at the ends and caution must be exercised in applying these values of A and B outside the parametric ranges covered in the experiment. The newly predicted jet trajectories along with the experimental data are shown in Figure 9.

The empirical formula determined by Muppidi and Mahesh also required the constants A and B. The values for these constants were also determined from the experimental data and best fit curves were generated to yield,

$$A = 0.0036\left(r^2\right) - 0.1226\left(r\right) + 2.3292 \tag{9}$$

and

$$B = 0.0898\ln\left(r\right) + 0.1971 \tag{10}$$

The values for A and B which match the experimental data along with the best-fit curves (Eqs. (9) and (10)) are shown in Figure 10. These equations accurately represent the jet trajectory and have an error less than 5 percent for all values of z/d. The newly predicted jet trajectories along with the experimental data are shown in Figure 11.

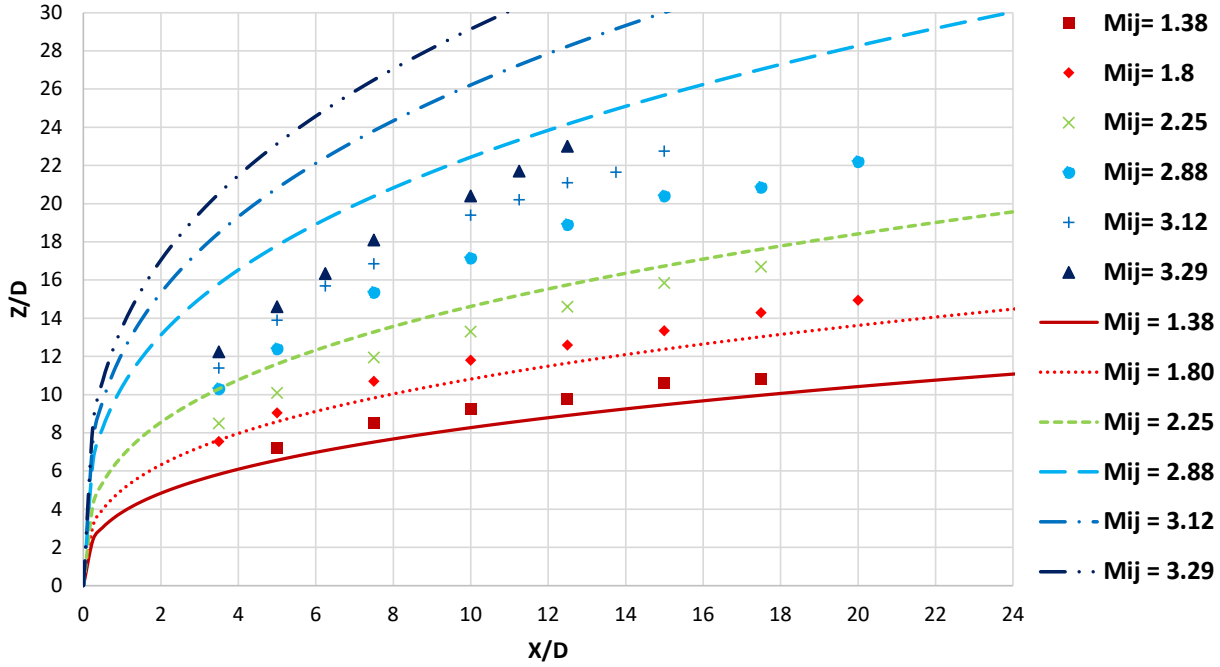

Figure 6.—Comparison of the predicted jet trajectory obtained from Abramovich (Ref. 10) (lines) and the experimental data (symbols).

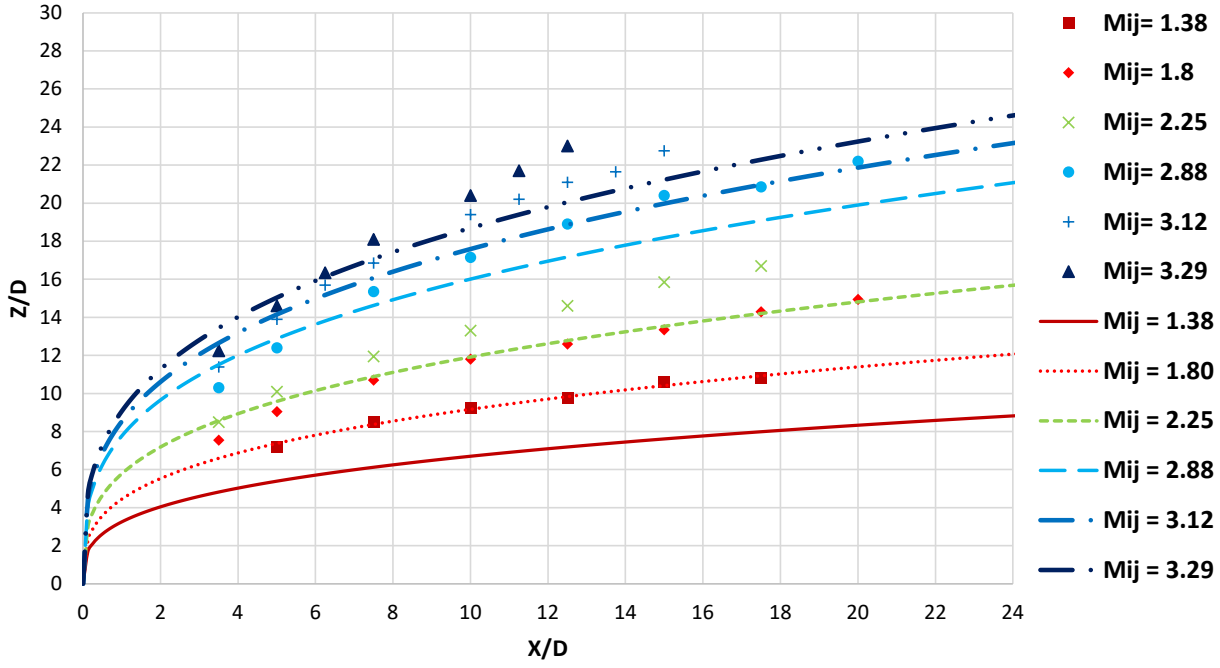

Figure 7.—Comparison of the predicted jet trajectory obtained from Karagozian (Ref. 11) (lines) and the experimental data (symbols).

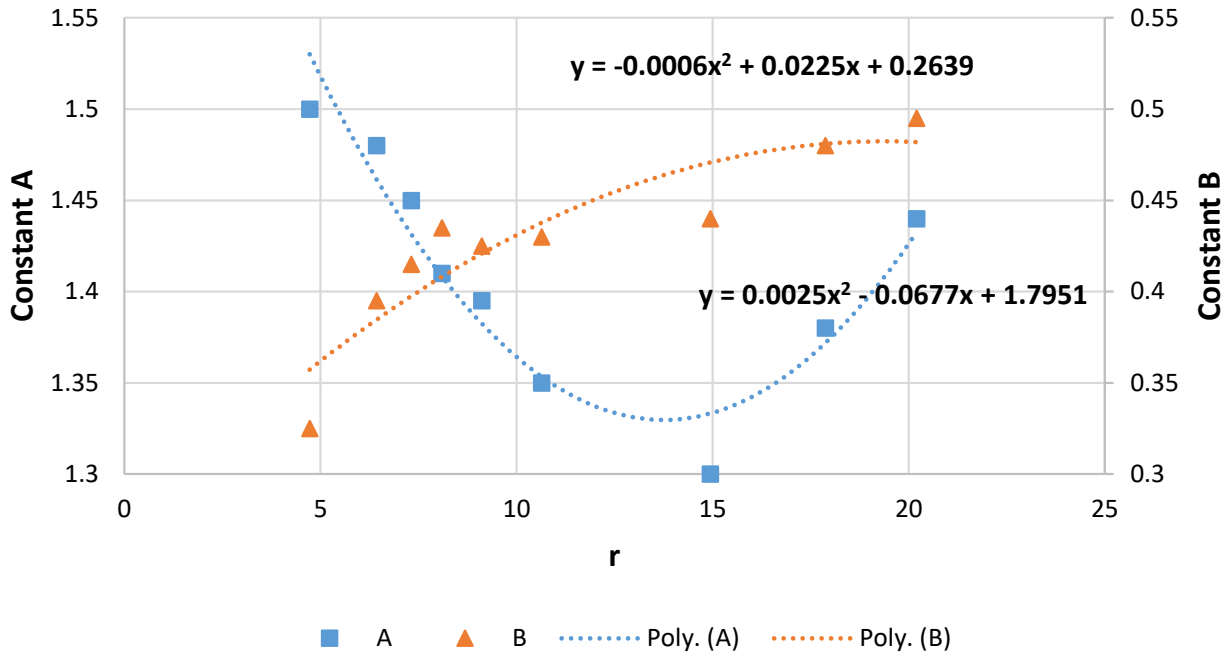

Figure 8.—Values for the constants *A* and *B* in the formulation of Broadwell and Breidenthal (Ref. 12) (Eq. (3)) obtained from the experimental data and best fit curves are shown as a function of velocity ratio *r*. (In legend equations, y = *A* or *B* and x = *r*).

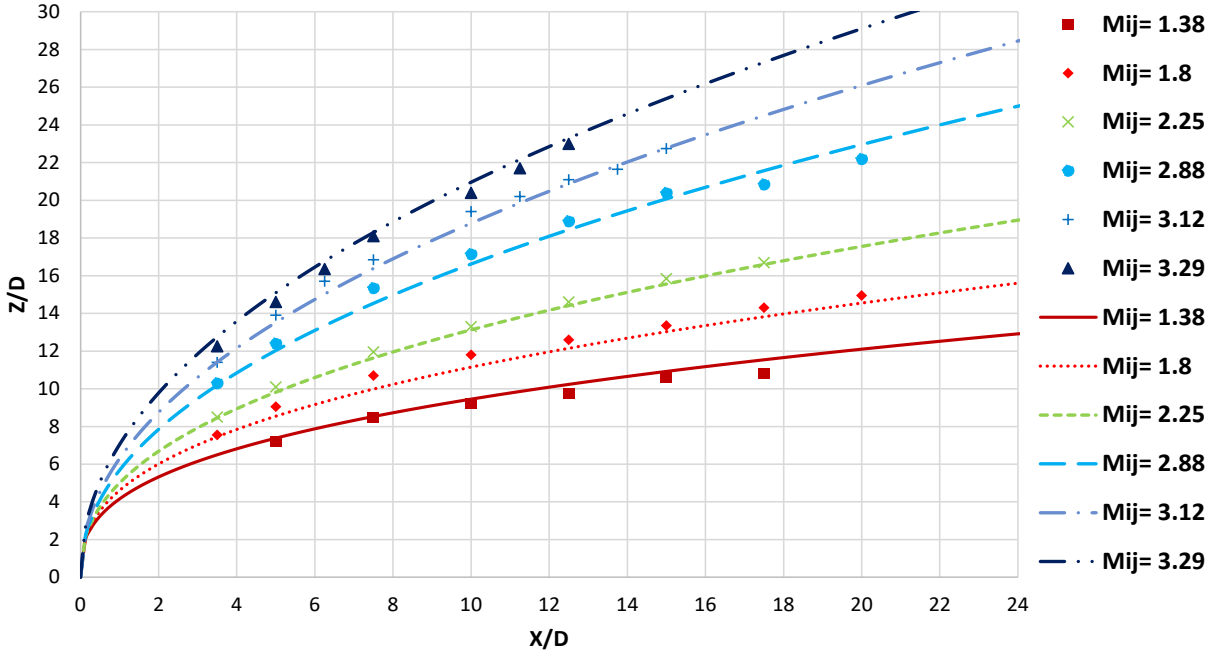

Figure 9.—Prediction by empirical formula of Broadwell and Breidenthal (Ref. 12), with currently adjusted values for *A* and *B*, shown by the lines compared to the experimental data (symbols).

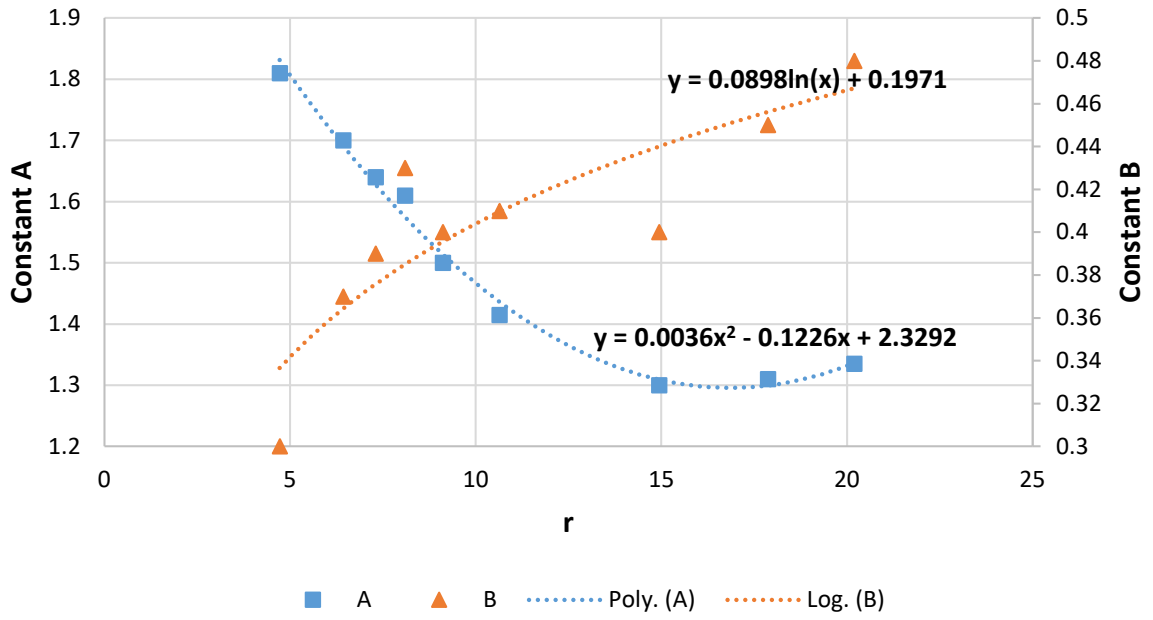

Figure 10.—Values for the constants *A* and *B* in the formulation of Muppidi and Mahesh (Ref. 14) obtained from the experimental data and best fit curves are shown as a function of velocity ratio *r*. (In legend equations, y = *A* or *B* and x = *r*).

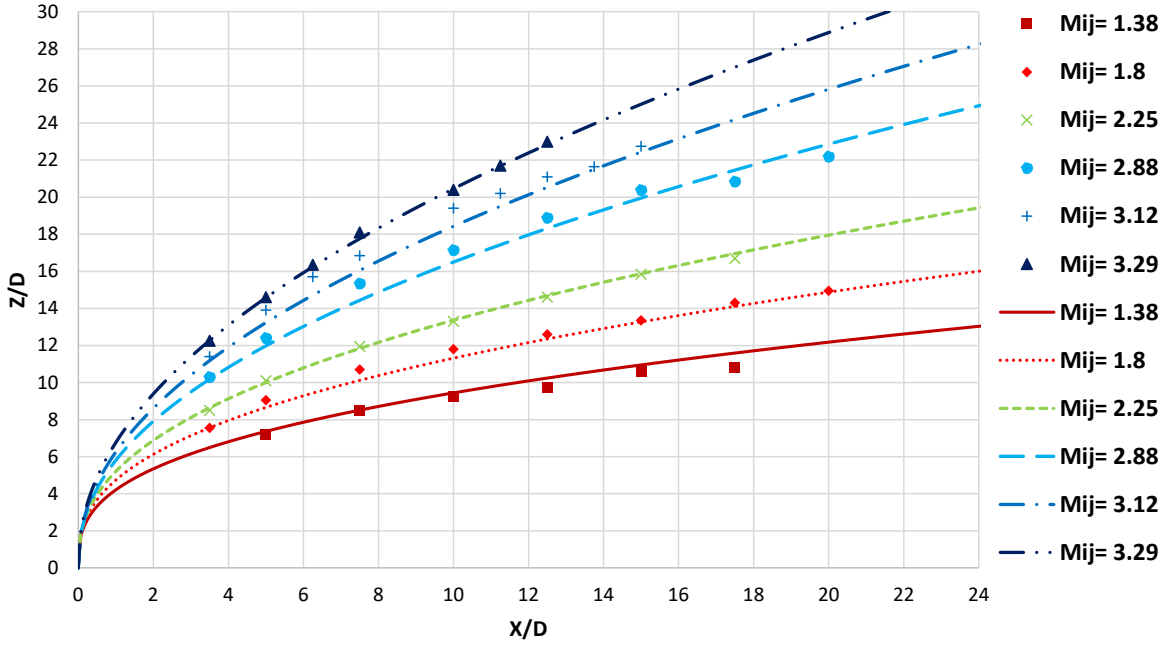

Figure 11.—Prediction by empirical formula of Muppidi and Mahesh (Ref. 14), with currently adjusted constants A and B, shown by the lines compared to the experimental data (symbols).

4.2 Numerical Results

This section presents the numerical results and compares them to the empirical and experimental results reported in Section 4.1. As stated before, the numerical results were obtained using (3-D) FUN3D analysis. Note that the adjoint method adds grids as the solution progresses, thus optimizing the grid density (Ref. 18). From the numerical solutions, the jet trajectories were obtained by locating the maximum velocities along the *z*-axis starting from the orifice up to 50*d* downstream.

Results obtained from FUN3D using the SA turbulence model are shown in Figure 12 for four injector jet Mach numbers (M_{ij} = 1.38, 2.25, 2.88, 3.29). As expected, when M_{ij} increases the injector jet penetration increases. A 'barrel shock', noticeable in Figure 12, becomes more prominent as M_{ij} increases. A bifurcation of the injector jet can also be observed. The reason for the bifurcation remains unclear. The convergence histories showed that the numerical solutions converged.

From the numerical results, the JICF trajectories were obtained and compared to the experimental data and the empirical formula developed by Muppidi and Mahesh (Figure 13). The empirical results shown use the values for constants A and B, determined experimentally, from Equations (9) and (10). The differences between the numerical and experimental results in Figure 13 increase with increasing M_{ij}. The numerical results are within 11 percent of the experimental values at M_{ij} = 1.38 but the difference increase to 65 percent at M_{ij} = 3.29. The jumps in the numerical data in the range x/d<2 are attributable to the 'barrel shock' (Figure 12).

The comparisons among the results for the four of FUN3D's turbulence models (SA, SA-Neg, SST, SST-V) at the lowest Mach number case, M_{ij} = 1.38, are shown in Figure 14. Attempts were made to acquire solutions from FUN3D's turbulence models SST, SST-V, and SA-Neg at higher Mach numbers but failed due to residual errors. The reason for this is not clear but might trace to the more complex shock structures and inherently unsteady nature of the flows. The results in Figure 14 show that at M_{ij} = 1.38 the four turbulence models produce similar results.

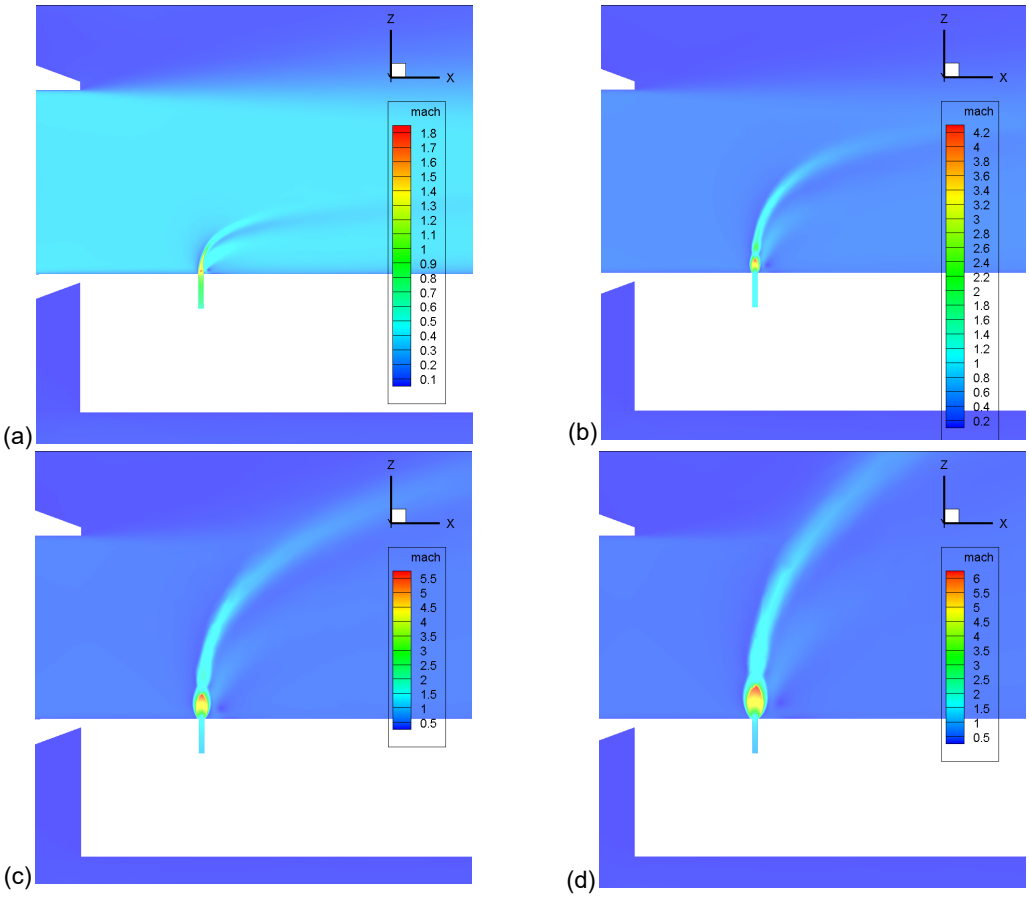

Figure 12.—Contour plots of the Mach number obtained from FUN3D numerical solutions. (a) Mij = 1.38, (b) Mij = 2.25, (c) Mij = 2.88, (d) Mij = 3.29.

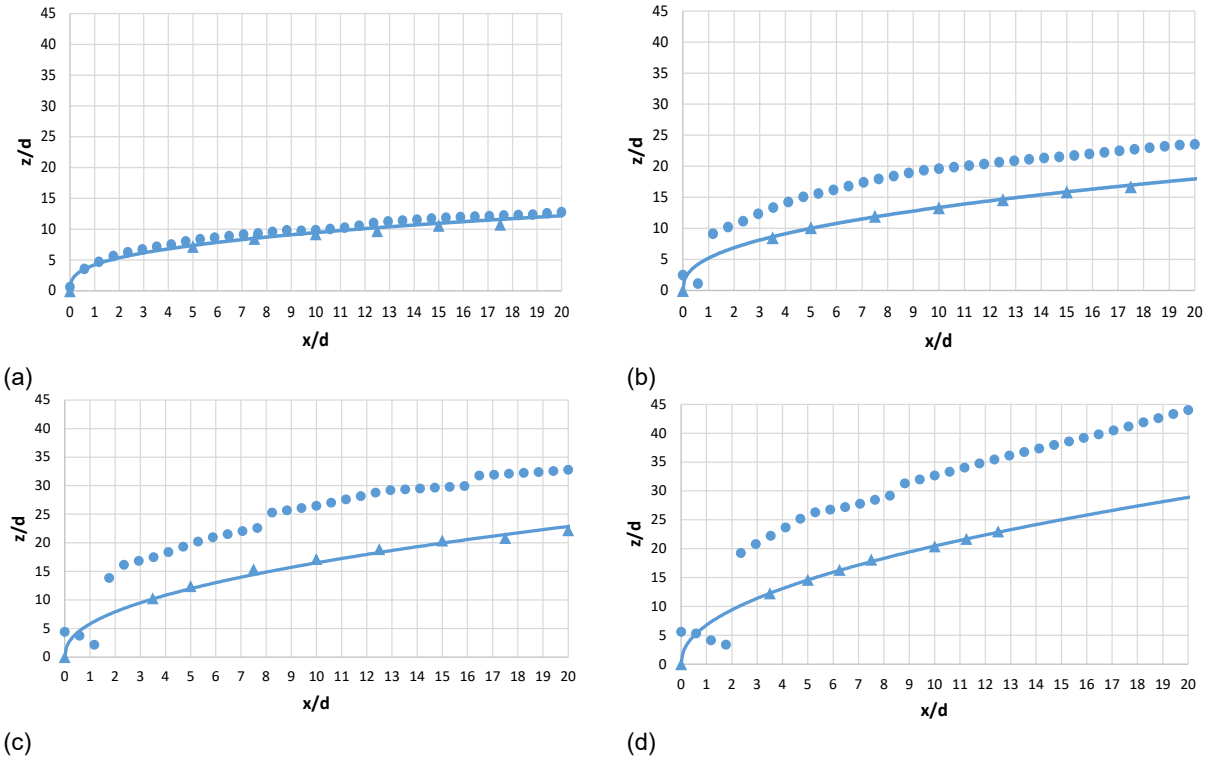

Figure 13.—Comparison of the trajectories obtained from FUN3D solution using the SA turbulence model (circles) and the empirical formula of Muppidi and Mahesh (Ref. 14) (line). Experimental data are indicated by triangles. The results are for M_{ij} of (a) 1.38, (b) 2.25, (c) 2.88, and (d) 3.29.

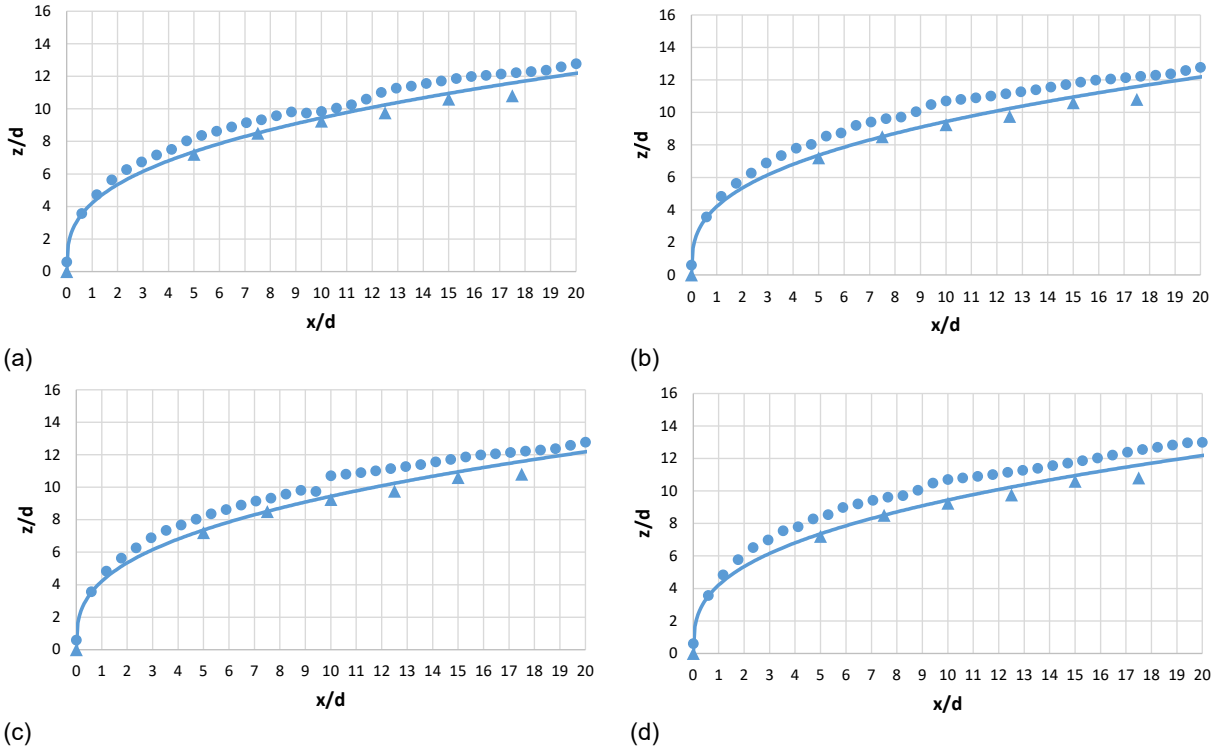

Figure 14.—Comparison of the trajectories obtained from the FUN3D solutions (circle's) and the empirical formula of Muppidi and Mahesh (Ref. 14) (line). Experimental data are indicated by triangles. The results are for M_{ij} = 1.38 and the (a) SA, (b) SST, (c) SA-Neg, and (d) SST-V turbulence models.

5.0 Summary

The comparisons between the experimental data and empirical formulae show that Abramovich's (Ref. 10) and Karagozian's (Ref. 11) formulae do not accurately predict the trajectories of highly underexpanded supersonic jets exhausting into subsonic crossflow. Broadwell and Breidenthal's (Ref. 12) and Muppidi and Mahesh's (Ref. 14) formulae also exhibit large deviations when the specified values for the constants A and B in their correlations are used. Probable reasons for these deviations are thought to be due to differences in flow conditions, the most significant effect being that of compressibility in the present study. Note that predictions from these previous studies, mostly conducted for incompressible flows, also differ from one another. Again, differences in flow conditions among those studies, namely, the injector nozzle geometry, mean velocity and turbulence characteristics at the nozzle exit, etc. might account for the differences. In this study, the values of A and B were determined from the experimental data. These values were curve fitted to express them as a function of the velocity ratio r. When these values are used, the difference between the experimental data and the predictions from the empirical formulae are less than 5 percent. The curve-fit equations for A and B are provided. It is emphasized that the fitted curves for A and B pertain to the parametric ranges covered in the experiment (M_{ij} range of 1.38 to 3.29 corresponding to r range of 5 to 20) and caution must be exercised in applying these values outside those ranges.

Numerical solutions obtained from FUN3D were compared to the experimental results. With the SA turbulence model, FUN3D provided the trajectories within 11 percent of the measured values at the lowest Mach number, $M_{ij} = 1.38$. The numerical results deviated significantly from the experimental results, up to 65 percent, at the highest Mach number, $M_{ij} = 3.29$. Some of the turbulence models with FUN3D also failed to produce converged solutions at higher Mach numbers. It is speculated that the differences with the data and the failures at higher Mach numbers could be due to more complex shock structures and inherent unsteadiness in the flows.

References

1. Zaman. K.B.M.Q., "Unsteady jets in crossflow," *ASME HT-FED2004-56822*, Heat Transfer/Fluids Engineering Summer Conference, Charlotte, NC, 11-15 July, 2004.
2. Beresh, S.J. and Henfling, J.F. and Erven, R.J. and Spillers, R.W., "Penetration of transverse supersonic jet into a subsonic compressible crossflow," *AIAA Journal*, vol. 43, no. 2, 2005.
3. Kamotani, Y. and Greber, I., "Experiments on turbulent jet in a crossflow: *AIAA J.* 10, 1425–1429, 1972.
4. Fearn, R.L. and Weston R.P., "Vorticity associated with a jet in crossflow," *AIAA J.* 12, 1666–1671, 1974.
5. Krothapalli, A., Lourenco, L. and Buchlin, J.M., "Separated flow upstream of a jet in a crossflow," *AIAA J.* 28, 414–420, 1990.
6. Kelso, R.M. and Smits, A.J., "Horseshoe vortex systems resulting from the interaction between a laminar boundary layer and a transverse jet," *Physics Fluids*, 7, 153–158, 1995.
7. Fric, T.F. and Roshko, A., "Vortical structures in the wake of a transverse jet," *J. Fluid Mechanics,* 279, pp. 1–47, 1994.
8. Foster, L.E. and Engblom, W.A., "Computation of transverse injection into supersonic crossflow with various injector orifice geometries," *AIAA Paper 2004-1199*, 42nd Aerospace Sciences Meeting and Exhibit, Reno, NV, 5-8 January, 2004.
9. Papamoschou, D. and Hubbard, "Visual observations of supersonic transverse jets," *Exp. Fluids* 14:468-76, 1993.

10. Ambramovich, “The Theory of Turbulent Jets. Massachusetts Institute of Technology,” 543–552, 1963.
11. Karagozian, A.R. “An analytical model for the vorticity associated with a transverse jet,” *AIAA Journal*. 24, 429–436, 1986.
12. Broadwell, J.E. and Breidenthal, R.E., “Structure and mixing of a transverse jet in incompressible flow,” *J. Fluid Mech*. 148, 405–412, 1984.
13. Margason, R.J., “Fifty years of jet in crossflow research,” In AGARD Symp. on a Jet in Cross Flow, Winchester, UK, AGARD CP-534, 1993.
14. Muppidi, S. and Mahesh, K., “Study of trajectories of jets in crossflow using direct numerical simulations,” *J. Fluid Mech.* 501. 81–100, 2005.
15. Tam, C.K.W. and Tanna, H.K., “Shock associated noise of supersonic jets from convergent-divergent nozzles,” *Journal of Sound and Vibration (1982) 81(3), 337–358*. Marietta, GA. 30 July, 1981.
16. Frate, F.C. and Bridges, J.E., “Extensible rectangular nozzle model system,” *AIAA Paper 2011-975*, 49th Aerospace Sciences Meeting, Orlando, Fl, 4–7 January, 2011.
17. Zaman, K.B.M.Q., “Flow-field surveys for rectangular nozzles,” *NASA TM-2012—217410* (see also *AIAA Paper 2012-0069*), 2012.
18. FUN3D Manual: 13.7 NASA/TM-20205010139 Corrected Copy, November 2020.